

## COMMUNICATION

# Ambient Hydrolysis Deposition of TiO<sub>2</sub> in Nanoporous Carbon and the Converted TiN/Carbon Capacitive Electrode

Cite this: DOI: 10.1039/x0xx00000x

Received 00th January 2012,  
Accepted 00th January 2012

DOI: 10.1039/x0xx00000x

www.rsc.org/

Xingfeng Wang,<sup>#a</sup> Vadivukarasi Raju,<sup>#a</sup> Wei Luo,<sup>a</sup> Bao Wang,<sup>a</sup> William F. Stickle<sup>b</sup>  
and Xiulei Ji<sup>\*a</sup>

Despite the considerable advances of deposition technologies, it remains a significant challenge to form conformal deposition on surface of nanoporous carbons. Here, we introduce a new ambient hydrolysis deposition method that employs and controls pre-adsorbed water vapor on nanoporous carbons to define the deposition of TiO<sub>2</sub>. We converted the deposited TiO<sub>2</sub> into TiN via a nitridation process. The metallic-TiN-coated porous carbon exhibits superior kinetic performance as an electrode in electrical double layer capacitors. The novel deposition method provides a general solution for surface engineering on nanostructured carbons, which may result in a strong impact on the fields of energy storage and other disciplines.

Nanoporous materials are at the heart of important applications, such as energy storage, catalysis, sensing, drug delivery, and separation.<sup>1-4</sup> However, these materials often fall short on providing needed functionalities due to a lack of desirable surface properties. Despite the advances in deposition methods, it remains a significant challenge to form controllable conformal deposition inside nanoporous materials at ambient conditions. Vapor deposition methods, such as chemical vapor deposition (CVD), thermal deposition, or e-beam deposition, do not meet the requirements due to their line-of-sight nature. Most conformal methods, such as electrodeposition,<sup>5,6</sup> electroless deposition,<sup>7,8</sup> and dip/spin coating,<sup>9</sup> provide no control at the scale of a few nanometers. As the state-of-the-art conformal deposition methods, atomic layer deposition (ALD)<sup>10-12</sup> and under potential deposition (UPD)<sup>13,14</sup> have yet to demonstrate general applicability inside nanoporous materials.

Herein, we introduce a new ambient hydrolysis deposition (AHD) methodology for coating metal oxides on nanoporous carbons. The AHD involves water adsorption in porous substrates and a subsequent hydrolysis inside “wet” substrates via a dry non-aqueous solution of precursors. As schematically depicted in Fig. 1A, the water adsorption step differentiates the AHD from the conventional sol-gel methods where water and hydrolysis precursors

encounter porous substrates at the same time.<sup>15-17</sup> Water adsorption on activated carbons has been experimentally and theoretically studied although the related mechanism is still not well understood.<sup>18-20</sup> Unfortunately, this phenomenon has never been utilized for ambient deposition purposes. We, for the first time, demonstrate that the scale of ambient deposition of TiO<sub>2</sub> can be controlled by manipulating the water adsorption in nanoporous carbons. We also converted the TiO<sub>2</sub>-deposited nanoporous carbon to TiN/carbon nanocomposite as an electrode for electrical double layer capacitors (EDLCs).

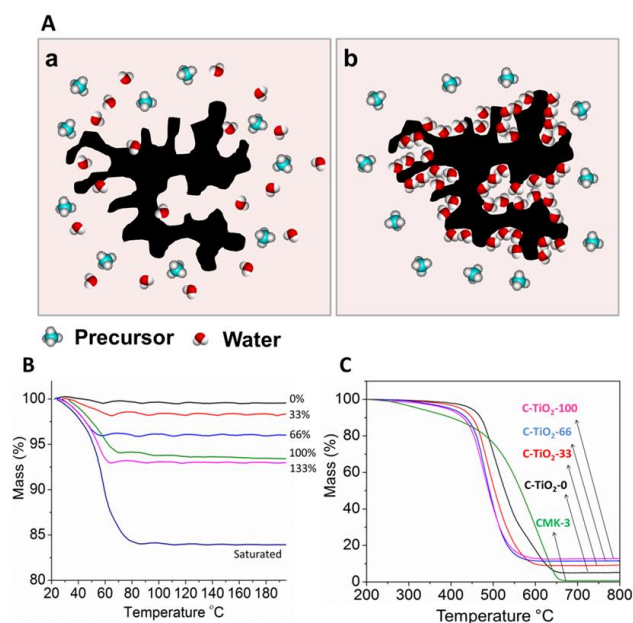


**Fig. 1.** A) Schematic showing the different water distribution between a) conventional sol-gel method and b) AHD method. B) TGA curves of C-APS with different levels of water loading. C) TGA curves of C-TiO<sub>2</sub> samples showing different levels of TiO<sub>2</sub> loading corresponding to water adsorption.

We chose CMK-3, a mesoporous carbon with a long-range ordered nanostructure (symmetry:  $P6mm$ ), as the model nanoporous carbon.<sup>21</sup> For the deposition composition, we selected  $\text{TiO}_2$  in this proof-of-concept study. In the first step of AHD, in order to increase the surface hydrophilicity for facile water vapor adsorption, CMK-3 is functionalized with carboxylic groups in a warm acidic ammonium persulfate (APS) solution. The obtained carbon is designated as C-APS. The number of carboxylic groups on C-APS was measured by Boehm titration to be 1.96 mmol/g. For water loading, we first exposed degassed C-APS to excessive saturation water vapor (80 °C) for one hour, and the adsorbed water was determined by thermogravimetric analysis (TGA) to be 16 wt%, as a reference. Then, a certain volume of saturation water vapor (80 °C) was measured by a syringe and exposed to the degassed C-APS contained in the same syringe (Fig. S1). By exposing C-APS to the water vapor volumes corresponding to molar ratios of 133%, 100%, 67%, and 33% of the reference water loading (16 wt%), 7.5 wt%, 7 wt%, 6 wt%, and 4 wt% of water were adsorbed, as revealed by the TGA results (Fig. 1B). These water-loaded carbons are referred to as C-133, C-100, C-67, and C-33, correspondingly. The results demonstrate that water loading in nanoporous carbon can be

**Table 1.** Physical characteristics of the samples.

Samples	$\text{TiO}_2$ (wt%)	Surface area ( $\text{m}^2/\text{g}$ )	Pore volume ( $\text{cc}/\text{g}$ )	Microporous	
				Surface area ( $\text{m}^2/\text{g}$ )	Pore volume ( $\text{cc}/\text{g}$ )
CMK-3	N.A	1233	1.59	176	0.08
C-APS	N.A	970	1.39	109	0.04
C- $\text{TiO}_2$ -0	5.2	792	1.09	184	0.09
C- $\text{TiO}_2$ -33	9.1	780	1.00	73	0.03
C- $\text{TiO}_2$ -67	11.3	757	0.94	62	0.02
C- $\text{TiO}_2$ -100	12.6	729	0.90	75	0.03
C-Ti-N	N.A	1078	1.21	188	0.08

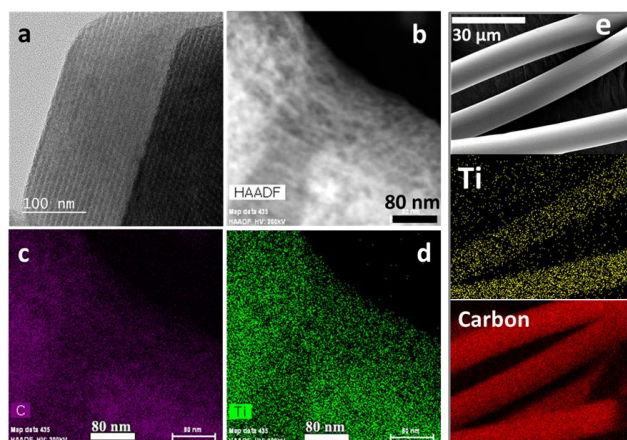


**Fig. 2.** Electron microscopy studies of C-APS and C- $\text{TiO}_2$ -100. a) A bright-field TEM image of C-APS. b) An HAADF-STEM image of C- $\text{TiO}_2$ -100. c,d) Carbon and titanium EDX mappings corresponding to the image in b. e) A SEM image of activated carbon, and the corresponding carbon and titanium EDX mappings.

controlled, which constitutes the foundation for the controllable AHD method. In the following step, water-loaded C-APS samples were soaked in the 1,3 dioxolane (DOXL) solution of titanium tetraisopropoxide (TTIP) (5 vol%) in an Argon-filled glovebox. The composites were collected by filtration and dried in an oven.

It is necessary to mark the minimum scale of deposition that is determined by the water from the DOXL solution of TTIP. Degassed C-APS was soaked in the precursor solution, and 5.2 wt% of  $\text{TiO}_2$  was loaded. Note that CMK-3 is nearly ash free. The obtained  $\text{TiO}_2/\text{C}$  nanocomposite is referred to as C- $\text{TiO}_2$ -0, where “0” indicates that no water is pre-adsorbed (Fig. 1C). With C-33, C-66 and C-100 as the substrates, the  $\text{TiO}_2$  loadings were 9.1 wt%, 11.3 wt%, and 12.6 wt%, respectively (Fig. 1C and Table 1).

We investigated the deposition uniformity of the AHD method by looking at C- $\text{TiO}_2$ -100 as the representative material. It is evident that C- $\text{TiO}_2$ -100 maintains a long-range ordered nanostructure comparable to that of C-APS, as revealed by the high-angle angular dark field scanning TEM image (HAADF-STEM). More importantly,  $\text{TiO}_2$  phase is uniformly distributed in the nanocomposite, as suggested by the corresponding titanium elemental mapping (Fig. 2a,b,d). We are aware of the fact that water and dioxolane are miscible to each other. However, the fact that  $\text{TiO}_2$  phases are successfully deposited inside pores of nanoporous carbon instead of being deposited on the particle surface indicates that the hydrolysis reaction in the pores is kinetically more favorable than water diffusion from the porous carbon framework to bulk dioxolane/precursor solution.

It has been a long-standing challenge to impregnate microporous carbons with an oxide deposition. With same AHD method, we successfully deposited  $\text{TiO}_2$  in an activated carbon that exhibits a high surface area of 2715  $\text{m}^2/\text{g}$  and an average pore size around 2.3 nm (Fig. S2). A representative SEM image with the corresponding titanium EDX mapping reveals the homogeneous  $\text{TiO}_2$  deposition (Fig. 2e). The activated carbon was prepared by activating a commercially available coal-derived carbon by  $\text{CO}_2$  oxidation (Supplementary information).

The wide-angle X-ray diffraction (XRD) pattern of C- $\text{TiO}_2$ -100 with no crystalline features confirms the small  $\text{TiO}_2$  particle sizes observed by TEM (Fig. S3). Table 1 summarizes the porosity

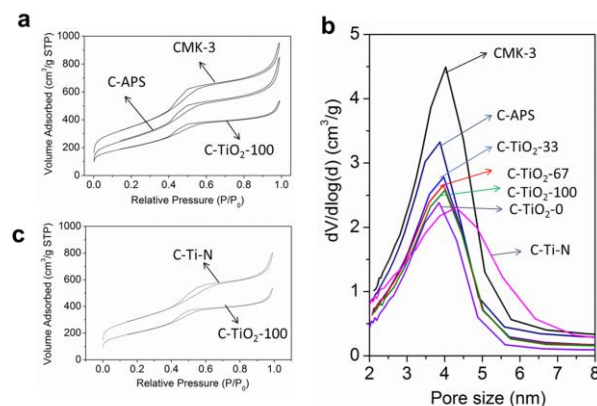


**Fig. 3.** a)  $\text{N}_2$  sorption isotherms of CMK-3, C-APS and C- $\text{TiO}_2$ -100. b) Pore size distributions of different samples. c) Isotherms of C- $\text{TiO}_2$ -100 and C-Ti-N. The results together with Table 1 reveal the distribution of hydrolysis-based deposition in C-APS.

characteristics of the samples. (See isotherms in Fig. 3a and S4). It is evident that the functionalization of carboxylic groups does affect the CMK-3 nanostructure. After the  $\text{TiO}_2$  deposition, the specific surface area and pore volume, particularly, the micropore characteristics were further diminished. The pore size distribution (PSD) of the C- $\text{TiO}_2$  samples slightly shifts to larger values, compared to that of C-APS (Fig. 3b). This indicates that the deposition primarily occurs in smaller mesopores or micropores in water-adsorbed C-APS. As known, water vapor is preferably adsorbed in smaller pores.<sup>18</sup> As the population of pores with smaller sizes decreases, the weight of the PSD of the C- $\text{TiO}_2$ -100 shifts to larger pore sizes. Note that the PSD of C- $\text{TiO}_2$ -100 is still within the envelope of the PSD of C-APS, and no larger pores are newly formed. This shift together with the diminished micropore features indicates that the sizes of the most deposited  $\text{TiO}_2$  nanodomains may range from dimensions below 2 nm to values between 3 to 4 nm. In sharp contrast, the micropore features of C- $\text{TiO}_2$ -0 were doubled after deposition, which suggests that the hydrolysis deposition in this case turned large mesopores into micropores. For C- $\text{TiO}_2$ -0, hydrolysis, water mainly comes from the precursor solution, and it is unfavorable for liquid water to reach smaller pores.

We have demonstrated that the AHD method enables ambient conformal deposition of  $\text{TiO}_2$  in nanoporous carbons. A great

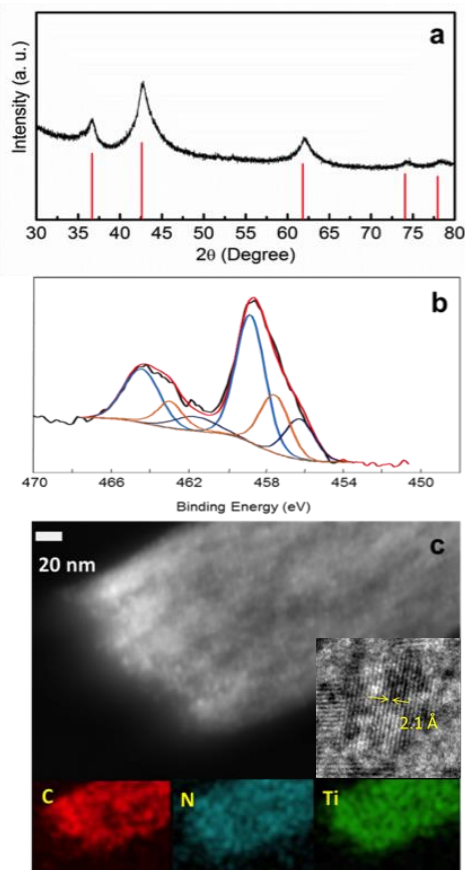


**Fig. 4.** Compositional and structural characterizations of C-TiN. a) XRD pattern. b) XPS Ti [2p] signal. c) HAADF-STEM and carbon, nitrogen and titanium EDX mappings. Inset: a representative HRTEM image of a TiN particle. The results reveal that TiN nanocrystallites are homogeneously dispersed in C-APS.

advantage of oxide deposition is that oxides can be potentially turned to other compositions by chemical reactions. We chose to convert  $\text{TiO}_2$  coating into TiN in C-APS as an electrode for enhanced rate performance in EDLCs. EDLCs operate on electrostatic interaction between polarized amorphous carbon surface and solvated ions.<sup>22-25</sup> The low conductivity of amorphous carbon limits the kinetic performance of EDLCs. Thus, graphitic innovative carbons, such as graphene-based electrodes,<sup>26-29</sup> have been investigated, demonstrating much improved power performance in EDLCs. Another approach is to improve the surface conductivity of carbon electrodes, and N-doping shows some effect.<sup>30-33</sup> We chose to form a TiN layer on porous carbon surface due to its high electrical conductivity ( $5 \times 10^6$  S/m), two orders higher than theoretical graphene, and good corrosion resistance.<sup>34-37</sup> C- $\text{TiO}_2$ -100, as the model composite, was annealed at 850 °C under  $\text{NH}_3$  for 6 hrs. We referred to the obtained composite as C-TiN. The XRD pattern of C-TiN depicts a single cubic phase of TiN (JCPDS 38-1420), and confirms the absence of crystalline  $\text{TiO}_2$  and TiON (Fig. 4a). The XRD pattern indicates a complete nitridation because any remained  $\text{TiO}_2$  or TiON would be crystallized at 850 °C and display crystalline peaks. The TiN coherence length is estimated by the Scherrer Equation to be 4.0 nm from the XRD peaks.

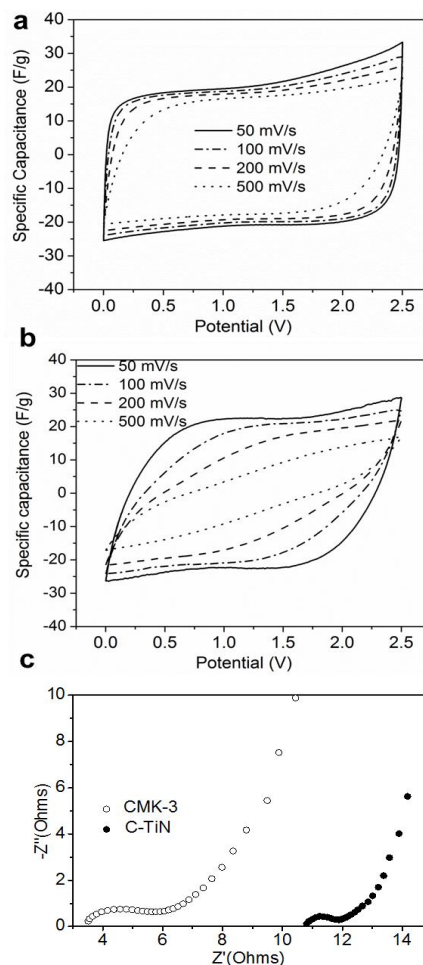


**Fig. 5.** a,b) CV curves at different scanning rates for C-TiN and CMK-3, respectively. c) Nyquist plots of C-TiN and CMK-3 electrodes.

To further identify the chemical compositions, we conducted X-ray photoelectron spectroscopy (XPS). The Ti 2p<sub>3/2</sub> peak of C-TiN can be deconvoluted into three components at 456.3 eV (TiN), 457.6 eV (TiON), and 458.8 eV (TiO<sub>2</sub>) (Fig. 4b). The combined XRD and XPS results suggest that the amorphous TiO<sub>2</sub> and TiON phases were inevitably formed during the sample handling.<sup>38</sup> The contribution of TiO<sub>2</sub> and TiON is certainly overestimated by XPS due to their overwhelming presence at particle surface. We further studied the structure of C-TiN by HAADF-STEM and the corresponding titanium EDX mapping, as shown in Fig. 4c. The HAADF-TEM image depicts the well-maintained nanostructure of CMK-3 with finely-dispersed nanoparticles. Revealed by a high resolution TEM image, the sizes of TiN nanocrystallites range from 3 to 5 nm with characteristic lattice fringes mostly oriented along the plane (200) (Fig. S5). A representative TiN nanoparticle with d-spacing of 2.1 Å is shown in Fig. 4 inset. As Table 1 summarizes, the porosity characteristics of C-TiN are larger than those of C-TiO<sub>2</sub>-100. Particularly, the specific pore volume and surface area of micropores were dramatically increased after nitridation, compared to C-TiO<sub>2</sub>-100. As shown in Fig. 3c, the isotherm hysteresis of C-TiN shifts to a higher relative pressure (P/P<sub>0</sub>) after nitridation, compared to C-TiO<sub>2</sub>-100. The PSD peak of C-TiN shifts to 4.3 nm from 3.9 nm, as shown in Fig. 3b. This may be caused by the TiN nanoparticle formation process at the expense of TiO<sub>2</sub> clusters that migrated out of the micropores. Note that the micropore surface area of C-TiN is even larger than C-APS. It seems that there might be a carbon oxidation/activation phenomenon during the nitridation process.

We compared the electrochemical performances of C-TiN and pristine CMK-3 as EDLC electrodes. A control sample, referred to as CMK-N, was prepared by the nitridation of C-APS. The pore size distributions of C-APS and CMK-N are presented in Fig. S6a, and the nitrogen content is determined to be ~3.2 at% by EDX (Fig. S6b). After the nitridation treatment of C-APS, the microporous characteristics completely disappeared, and a bimodal structure was formed with additional bigger pores peaked at ~9 nm. Cyclic voltammetry (CV) measurements were conducted at different scanning rates of 50, 100, 200, and 500 mV/s. As Figure 5a shows, C-TiN maintains the rectangular shape very well in its CV curves even at 500 mV/s, and area enclosed in CV curves does not shrink much upon higher scanning rates. Similar phenomenon was also observed on nanoporous graphene electrode.<sup>27</sup> In sharp contrast, the CV curves of CMK-3 are almost flattened upon high scanning rates (Fig. 5b), and similar CV results were observed for CMK-N, as shown in Fig. S7. Fig. S8 shows the galvanostatic charge and discharge profiles of CMK-3 and C-TiN at different current rates. The two materials exhibit similar capacitance values but vastly different equivalent series resistance (ESR). For example, at the current rate of 0.5 A/g, the ESR is 21.9 Ω and 118 Ω for C-TiN and CMK-3, respectively. Figure 5c shows the Nyquist plots obtained at the frequency range from 200 kHz to 10 mHz, where C-TiN exhibits a smaller semicircle compared to CMK-3 (1 Ω vs. 2 Ω), indicating a lower electrode/electrolyte interface resistance for C-TiN than CMK-3. The high ohmic resistance of C-TiN may be due to the oxidation process in forming C-APS. It has been clearly demonstrated that the TiN coating significantly improves the kinetic response of the electrode although some TiO<sub>2</sub> and TiON phases are formed on the surface of TiN nanocrystallites, and the rate improvement is certainly not from the N-doping effect.

In summary, we have demonstrated a new ambient hydrolysis deposition methodology to coat TiO<sub>2</sub> onto nanoporous carbons. The novel approach can tune the hydrolysis scales by varying the levels of pre-adsorbed water inside the porous carbon. To the best of our knowledge, this is the first ambient deposition method for nanoporous materials. It is potentially scalable due to its simplicity and low cost. Furthermore, we converted deposited TiO<sub>2</sub> into TiN nanocrystallites on the carbon surface by an NH<sub>3</sub>-based nitridation process to improve the surface conductivity of the nanoporous carbon electrodes in EDLCs. The TiN phase greatly improves rate performance, which unequivocally demonstrates that metallizing surface of amorphous carbon electrodes is a viable approach for enhanced EDLCs. Please note that it is not our intention in this article to provide electrode materials that is mature enough for next generation supercapacitors. We simply hope to point out by our results that a poorly conductive porous carbon can be turned into high-rate electrode materials in supercapacitors by the AHD coating and the following surface metallizing treatment.

## Acknowledgements

This research is financially supported by Oregon State University (OSU). We are grateful to Ms. Teresa Sawyer and Dr. Peter Eschbach for their help in SEM and TEM measurements in OSU EM Facility, funded by National Science Foundation, Murdock Charitable Trust and Oregon Nanoscience and Microtechnologies Institute. We are thankful to Mr. Joshua Razink in the CAMCOR Facility at University of Oregon for his HRTEM measurements.

## Notes and references

<sup>a</sup> Oregon State University, Department of Chemistry, Corvallis, Oregon, 97331. E-mail: [david.ji@oregonstate.edu](mailto:david.ji@oregonstate.edu)

<sup>b</sup> Hewlett-Packard Co., Corvallis, Oregon.

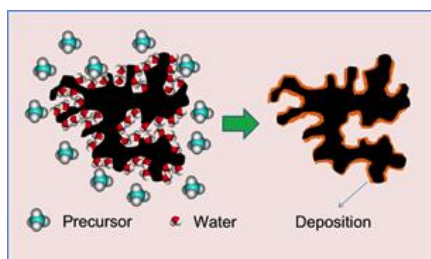
<sup>#</sup> These authors contributed equally to this work.

† Electronic Supplementary Information (ESI) available: [Experimental part and Figures available]. See DOI: 10.1039/c000000x/

- X. Feng, G. E. Fryxell, L. Q. Wang, A. Y. Kim, J. Liu, K. M. Kemner *Science* 1997, **276**, 923-926.
- Z. Tan, Z. Sun, H. Wang, Q. Guo, D. Su, *J. Mater. Chem. A*, 2013, **1**, 9462-9468.
- Z. Sun, L. Wang, P. Liu, S. Wang, B. Sun, D. Jiang, F.-S. Xiao, *Adv. Mater.*, 2006, **18**, 1968-1971.
- Z. Tan, Z. Sun, Q. Guo, H. Wang, D. Su, *J. Mater. Sci. Technol.*, 2013, **29**, 609-612.
- M. Datta, *Electrochim. Acta* 2003, **48**, 2975-2985.
- V. Dublin, K. Hong, N. Baxter, *US Pat.*, 6893550, 2005.
- V. P. Menon, C. R. Martin, *Anal. Chem.* 1995, **67**, 1920-1928.
- M. Schlesinger, M. Paunovic, *Modern Electroplating*, John Wiley & Sons, New Jersey, 5th ed., 2010.
- S. T. Meyers, J. T. Anderson, D. Hong, C. M. Hung, J. F. Wager, D. A. Keszler, *Chem. Mater.* 2007, **19**, 4023-4029.
- C. Marichy, M. Bechelany, N. Pinna, *Adv. Mater.* 2012, **24**, 1017-1032.
- J. W. Elam, D. Routkevitch, P. P. Mardilovich, S. M. George, *Chem. Mater.* 2003, **15**, 3507-3517.

- 12 D. M. King, J. A. Spencer, X. Liang, L. F. Hakim, A. W. Weimer, *Surf. Coatings Tech.* 2007, **201**, 9163-9171.
- 13 L. B. Sheridan, D. K. Gebregziabihier, J. L. Stickney, D. B. Robinson, *Langmuir* 2013, **29**, 1592-1600.
- 14 L. P. Colletti, B. H. Flowers, Jr., J. Stickney, *J. Electrochem. Soc.* 1998, **145**, 1442-1449.
- 15 Y. Wan, H. Yang, D. Zhao, *Acc. Chem. Res.* 2006, **39**, 423-432.
- 16 B. Tian, X. Liu, H. Yang, S. Xie, C. Yu, B. Tu, D. Zhao, *Adv. Mater.* 2003, **15**, 1370-1374.
- 17 L. Zhang, C. M. B. Holt, E. J. Lubber, B. C. Olsen, H. Wang, M. Danaie, X. Cui, X. Tan, V. W. Lui, W. P. Kalisvaart, D. Mitlin, *J. Phys. Chem. C* 2011, **115**, 24381-24393.
- 18 A. Striolo, A. A. Chialvo, P. T. Cummings, K. E. Gubbins, *Langmuir* 2003, **19**, 8583-8591.
- 19 T. Ohba, H. Kanoh, K. Kaneko, *J. Am. Chem. Soc.* 2004, **126**, 1560-1562.
- 20 F. Cailliez, M. Trzpit, M. Soulard, I. Demachy, A. Boutin, J. Patarin, A. H. Fuchs, *Phys. Chem. Chem. Phys.* 2008, **10**, 4817-4826.
- 21 S. Jun, S. H. Joo, R. Ryoo, M. Kruk, M. Jaroniec, Z. Liu, T. Ohsuna, O. Terasaki, *J. Am. Chem. Soc.* 2000, **122**, 10712-10713.
- 22 P. Simon, Y. Gogotsi, *Nature Mater.* 2008, **7**, 845-854.
- 23 L. Wei, M. Sevilla, A. B. Fuertes, R. Mokaya, G. Yushin, *Adv. Energy Mater.* 2011, **1**, 356-361.
- 24 P. Simon, Y. Gogotsi, *Acc. Chem. Res.* 2013, **46**, 1094-1103.
- 25 M. Noked, A. Soffer, D. Aurbach, *J. Solid State Electrochem.* 2011, **15**, 1563-1578.
- 26 J. R. Miller, R. A. Outlaw, B. C. Holloway, *Science* 2010, **329**, 1637-1639.
- 27 Y. Zhu, S. Murali, M.D. Stoller, K.J. Ganesh. W. Cai, P. J. Ferreira, A. Pirkle, R. M. Wallace, K. A. Cychosz, M. Thommes, D. Su, E. A. Stach, R. S. Ruoff, *Science* 2011, **332**, 1537-1541.
- 28 M. F. El-Kady, V. Strong, S. Dubin, R. B. Kaner, *Science* 2012, **335**, 1326-1330.
- 29 H. Cheng, Z. Dong, C. Hua, Y. Zhao, Y. Hu, L. Qu, N. Cheng, L. Dai, *Nanoscale* 2013, **5**, 3428-3434.
- 30 Z. Wen, X. Wang, S. Mao, Z. Bo, H. Kim, S. Cui, G. Lu, X. Feng, J. Chen, *Adv. Mater.* 2012, **24**, 5610-5616.
- 31 L. Zhao, L. Z. Fan, M. Q. Zhou, H. Guan, S. Qiao, M. Antonietti, M. M. Titirici, *Adv. Mater.* 2010, **22**, 5202-5206.
- 32 S. L. Candelaria, B. B. Garcia, D. Liu, G. Cao, *J. Mater. Chem.* 2012, **22**, 9884-9889.
- 33 L. Qie, W. Chen, H. Xu, X. Xiong, Y. Jiang, F. Zou, X. Hu, Y. Xin, Z. Zhang, Y. Huang, *Energy Environ. Sci.* 2013, **6**, 2497-2504.
- 34 D. C. Higgins, J. Y. Choi, J. Wu, A. Lopez, Z. Chen, *J. Mater. Chem.*, 2012, **22**, 3727-3732.
- 35 X. Liu, Y. Zhang, T. Wu, J. Huang, *Chem. Commun.* 2012, **48**, 9992-9994.
- 36 D. Choi, P. N. Kumta, *J. Electrochem. Soc.* 2006, **153**, A2298-A2303.
- 37 X. Lu, G. Wang, T. Zhai, M. Yu, S. Xie, Y. Ling, C. Liang, Y. Tong, Y. Li, *Nano Lett.* 2012, **12**, 5376-5381.
- 38 M. Zukalova, J. Prochazka, Z. Bastl, J. Duchoslav, L. Rubacek, D. Havlicek, L. Kavan, *Chem. Mater.* 2010, **22**, 4045-4055.

## Table of Contents entry:



A new ambient hydrolysis deposition method employs and controls pre-adsorbed water to define the sequential hydrolysis deposition of TiO<sub>2</sub>.